Imaging Local Polarization in Ferroelectric Thin Films by Coherent X-Ray Bragg Projection Ptychography

S. O. Hruszkewycz, M. J. Highland, M. V. Holt, Dongjin Kim, C. M. Folkman, Carol Thompson, A. Tripathi, G. B. Stephenson, Seungbum Hong, and P. H. Fuoss

Phys. Rev. Lett. **110**, 177601 — Published 25 April 2013

DOI: 10.1103/PhysRevLett.110.177601

Imaging local polarization in ferroelectric thin films by coherent x-ray Bragg projection ptychography

S. O. Hruszkewycz,[1] M. J. Highland,[1] M. V. Holt,[2] Dongjin Kim,[1,3] C. M. Folkman,[1] Carol Thompson,[4] A. Tripathi,[5] G. B. Stephenson,[1,6] Seungbum Hong,[1,7,3] and P. H. Fuoss[1]

[1]*Materials Science Division, Argonne National Laboratory, Argonne, Illinois 60439, USA*
[2]*Center for Nanoscale Materials, Argonne National Laboratory, Argonne, Illinois 60439, USA*
[3]*Department of Materials Science and Engineering, KAIST, Daejeon 305-701, Korea*
[4]*Department of Physics, Northern Illinois University, DeKalb, Illinois 60115, USA*
[5]*School of Physics, The University of Melbourne, Parkville, Victoria 3010, Australia*
[6]*Advanced Photon Source, Argonne National Laboratory, Argonne, Illinois 60439 USA*
[7]*Nanoscience and Technology Division, Argonne National Laboratory, Argonne, Illinois 60439, USA*

(Dated: April 2, 2013)

We used x-ray Bragg projection ptychography (BPP) to map spatial variations of ferroelectric polarization in thin film $PbTiO_3$, which exhibited a striped nanoscale domain pattern on a high-miscut (001) $SrTiO_3$ substrate. By converting the reconstructed BPP phase image to picometer scale ionic displacements in the polar unit cell, a quantitative polarization map was made that was consistent with other characterization. The spatial resolution of 5.7 nm demonstrated here establishes BPP as an important tool for nanoscale ferroelectric domain imaging, especially in complex environments accessible with hard x-rays.

PACS numbers: 77.80.Dj, 61.05.cp, 42.30.Rx, 68.37.Yz

Quantitative high-resolution characterization of ferroelectric domains in single crystal films is key to understanding local behavior in ferroelectric materials at nanometer length scales [1]. Thin film ferroelectric stripe domains, for example, are governed by the energetic balance and coupling of strain, interfacial compensation, and polarization, making their properties highly tunable at length scales and in environments that make characterization challenging. Though ensemble scattering [2], electron imaging [3, 4], and scanning probe techniques [5, 6] have uncovered many fundamental properties of nanoscale ferroelectric domains, a means of imaging local domain polarization and morphology in complex environments and in buried device-like architectures has yet to be demonstrated. In this work, we used hard x-ray focused-beam Bragg projection ptychography (BPP) [7] to image 180° ferroelectric stripe domains in a $PbTiO_3$ thin film by quantifying out-of-plane polarization with sub-10 nm spatial resolution, enabling nondestructive imaging of ferroelectric domains under realistic boundary conditions.

In epitaxial ferroelectric thin films, polarization orientation and domain structures are strongly influenced by both interfacial strain [8] and electrical boundary conditions [9]. Here, we investigated a 25-nm-thick epitaxial film of $PbTiO_3$ grown by metalorganic chemical vapor deposition [10] on a single crystal (001) $SrTiO_3$ substrate with a 1° surface miscut along the [100] azimuth. The compressive strain in the film due to lattice mismatch with the substrate promotes the formation of polarization normal to the film plane at temperatures below the Curie temperature [8]. The resulting depolarizing field is cancelled on the macroscopic scale by the spontaneous formation of nanoscale 180° stripe domains with polarization orientation alternating into and out of the film, having predictable sizes and polar properties [2, 11, 12]. Additionally, $PbTiO_3$ stripe domain patterns are influenced by the $SrTiO_3$ substrate surface features such as step edges [13]. The film studied in this work was grown to have a thickness such that the equilibrium stripe domain period ($\Lambda \sim 19$ nm) [12] corresponded roughly to the mean terrace spacing of the miscut $SrTiO_3$ substrate surface (~ 22.4 nm). As a result, the predominant stripe direction was along the [010] direction, normal to the substrate miscut direction. With approximately one stripe period per average substrate surface terrace, the film was found to be kinetically stable in the stripe phase [2, 11, 12], allowing for the room temperature characterization of polar stripe domains in $PbTiO_3$ by conventional x-ray diffraction, focused x-ray Bragg projection ptychography, and piezoresponse force microscopy (PFM).

X-ray diffraction has been used to characterize the average properties of ferroelectric thin films in this and other systems by analyzing crystal truncation rods (CTRs) and diffuse Bragg scattering, from which film polarization and average in-plane domain characteristics can be determined [2, 12, 14]. In this work, both average and spatially resolved synchrotron x-ray measurements were made using the Hard X-ray Nanoprobe beamline [15, 16] after annealing the film in the stripe phase [17]. During the measurements, the sample was held under vacuum in the Nanoprobe chamber (1.8×10^{-5} Torr) and oriented such that the substrate miscut azimuth was normal to the scattering plane. The room temperature 00L specular CTR measured with a 0.5×0.5 mm unfocussed x-ray beam is shown in Fig. 1(a). From the position of the 002 $PbTiO_3$ film peak relative to the 002 $SrTiO_3$ substrate peak, the average out-of-plane c-lattice parameter of the tetragonal $PbTiO_3$ unit cell was determined to be 4.123 Å. This lattice parameter is consistent with previous measurements of this system and corresponds to an average out-of-plane polarization magnitude of 0.69 C/m^2 in the film [11].

After the $PbTiO_3$ 002 Bragg peak position was determined,

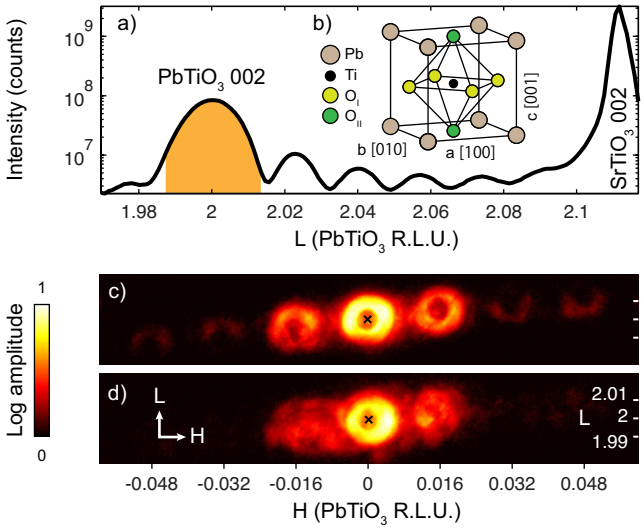

FIG. 1. (a) The 00L CTR containing the 002 Bragg peaks of the $PbTiO_3$ film and the underlying $SrTiO_3$ substrate measured with an unfocused x-ray beam. The shaded region of the $PbTiO_3$ peak corresponds to the angular divergence of the zone plate focusing optic. (b) The cubic perovskite $PbTiO_3$ unit cell structure. (c),(d) Coherent diffraction patterns taken with the focused beam illuminating 180° ferroelectric stripe domains. The x marks the position of the $PbTiO_3$ Bragg peak. (10 second exposures.)

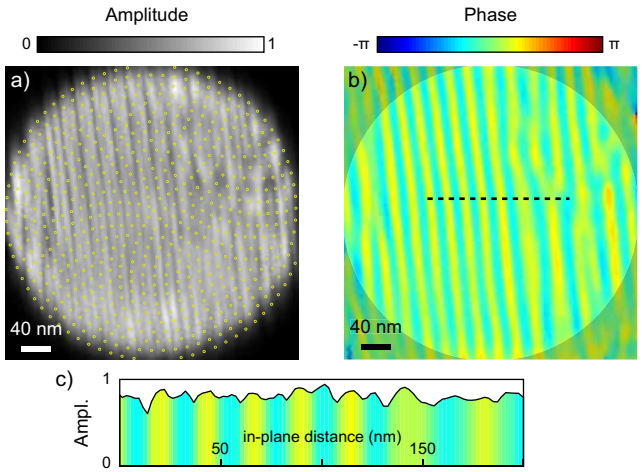

FIG. 2. (a) The amplitude of the BPP reconstructed $PbTiO_3$ thin film projection is shown in grayscale along with the raster positions of the beam (yellow dots). (b) The corresponding phase of the reconstruction. (c) A line through the reconstruction (along the dotted line in (b)) plotting reconstructed object amplitude colored by the corresponding pixel phase.

a hard x-ray zone plate focusing optic (numerical aperture of 2 mrad at the photon energy of 9.5 keV) was inserted into the beam to form a non-gaussian focus with a 40 nm full width at half maximum and intensity shoulders that spread the beam to 100 nm full width at quarter maximum. The focused beam was used to measure coherent Bragg nanodiffraction patterns from different regions of the film. Typical patterns from two regions are shown in Figs. 1(c) and (d), in which the center of the $PbTiO_3$ 002 Bragg peak is marked with an x. As shown in Fig. 1(a), the Bragg peak from the thin film is broad enough to diffract almost the full range of incident angles, so the diffracted beam replicates the annulus of angles produced by the incident optics (zone plate and central stop), modulated in L by the intensity profile of the $PbTiO_3$ film peak. The annular peak shape is characteristic of specular thin film diffraction from a zone plate with a central stop [7, 18]. Along the in-plane H direction, satellite peaks are clearly visible, spaced by 0.016 reciprocal lattice units (RLU). From the average spacing of the satellites measured with the unfocused parallel beam, the mean in-plane stripe period was determined to be $\Lambda = 22.9$ nm, closely matching the 22.4 nm average substrate terrace spacing.

Under coherent x-ray illumination conditions, an area Bragg diffraction pattern is the square of the Fourier amplitude of the electron density in the illuminated volume projected along the exit beam direction [19]. Regions of the film in which stripe domains are regularly spaced over tens of nanometers generate coherent nanodiffraction patterns like the one in Fig. 1(c), displaying well-defined first, second, and third order satellite peaks. By contrast, nanoscale illuminated regions with a less ordered stripe arrangement generate coherent diffraction patterns like the one shown in Fig. 1(d), with irregular speckled coherent diffraction. Only diffracted x-ray intensities were measured, so the real-space domain structures corresponding to these diffraction patterns cannot be directly determined by Fourier transform. However, with a set of Bragg nanodiffraction patterns that are appropriately sampled in real and reciprocal space, the phase problem can be iteratively solved, and a projection of the diffracting features in the film that give rise to the observed scattering can be reconstructed with Bragg projection ptychography [7].

For ptychographic imaging, coherent nanodiffraction patterns were collected at the $PbTiO_3$ 002 Bragg peak in a spiral pattern [20], scanning in the plane of the zone plate with an approximate point separation of 13 nm. The 650 scan points, spanning a circular region 390 nm in diameter, are shown as yellow points in Fig. 2(a). We used a combination of focused beam calculations [7, 21] and phasing algorithms [22, 23] to reconstruct a projection of the diffracting stripe domains in the $PbTiO_3$ film. (For details on BPP reconstruction procedures, see Reference [7].) The reconstructed amplitude and phase of the projected film in the scanned field of view are shown in Figs. 2(a) and (b). In the object reconstruction, the phase shows the domain morphology in the $PbTiO_3$ film, and the amplitude represents the diffracting electron density in the scanned field of view, but also contains stripe-like features. For constant-amplitude objects with sharp phase features (as in this case), low-signal counting statistics have been shown to produce errors in the reconstructions at high spatial frequencies [24]. Thus, the depressions in the amplitude in this reconstruction are likely errors due to the mixing of the real and imaginary components of the object, leading to the observa-

tion of phase-like structure in the modulus [24]. However, we note that the reconstructed amplitude remains relatively constant in the scanned field of view (10 % RMS, Fig. 2(c)) as expected for a continuous thin film with a homogeneously diffracting electron density. Therefore, the remaining discussion will focus on establishing the physical origin of the reconstructed phase in Fig. 2(b) and linking it quantitatively to the out-of-plane polarization distribution.

Bragg coherent x-ray diffraction imaging (CXDI) techniques, including BPP, map nanoscale spatial variations of the structure factor F_{HKL} in crystalline samples. The complex structure factor defines the amplitudes and phases of Bragg diffraction from a crystal unit cell, and is given by [25]:

$$F_{HKL} = \sum_n f_n e^{i2\pi(Hx_n + Ky_n + Lz_n)} \quad (1)$$

where f_n is the atomic form factor, $H\ K\ L$ are the reciprocal space lattice coordinates of a Bragg peak, and $x\ y\ z$ are the real space positions of atoms in the unit cell. At certain Bragg conditions, subtle local changes in the positions and internal structure of the unit cells will spatially modulate F_{HKL}, and that information becomes encoded in the coherent speckle about the Bragg peak. CXDI translates this information from reciprocal to real space, resulting in maps of the F_{HKL}. For crystals in which F_{HKL} is predominantly modulated by internal strain fields, a formalism has been established to quantitatively convert reconstructed phase into a scalar component of the local strain tensor [26]. While this formalism has been used to image and analyze internal strain in many different nanoscale crystals [26, 27], it is not applicable when F_{HKL} is predominantly modulated by non-uniform ionic displacements within the unit cell, as in stripe domains in a displacive perovskite ferroelectric crystal.

A $PbTiO_3$ crystal in the ferroelectric phase has a structure characterized by picometer-scale displacements of ions away from their centrosymmetric positions along the elongated tetragonal axis [28]. These ionic displacements give rise to a spontaneous polarization in the material. In this experiment, an in-plane compressive film strain state orients the polar axis along the film normal such that the elongated c-axis and the ionic displacements are largely parallel to the $\mathbf{G_{002}}$ scattering vector of the specular 002 $PbTiO_3$ Bragg peak. Since the ionic displacements and scattering vector have almost no in-plane components, spatial variations in F_{002} are primarily due to changes in z_n, the out-of-plane ion positions. These periodic structure factor modulations give rise to the pronounced in-plane coherent scattering seen in Fig. 1, and they were subsequently reconstructed with BPP. By linking F_{002} to Δz_n (the ionic displacements along z from the centrosymmetric, non-polar structure), the reconstructed BPP image can be interpreted in terms of local atomic structure and ultimately, polarization.

To relate the diffracted phase to local polarization, we need to know not only the displacements of the ions within a unit cell but also the displacements of the unit cells due to polarization gradients, e.g. across a 180° domain wall. These displacements have been calculated using *ab initio* theory [29]. Schematics of oppositely polarized unit cells corresponding to ideally compensated bulk $PbTiO_3$ are shown in Figs. 3(a) and (c) as they would appear on either side of a 180° stripe domain boundary. We assume that all displacements Δz_n scale with the local polarization, which can be calculated by summation of Born effective charges [30, 31]. The 002 unit cell structure factor calculated using Eq. (1) is plotted in Fig. 3(e) in terms of amplitude $|F_{002}|$ and phase $\angle F_{002}$, taking into account energy-dependent anomalous scattering contributions. For oppositely polarized domains with equal polarization magnitudes $|P|$, the structure factor magnitudes are nearly equivalent at 9.5 keV [32, 33], whereas the phases differ by as much as 1.5 radians. Thus, a mostly uniform amplitude is expected in the BPP reconstruction with stripes of alternating phase $\angle F_{002}$.

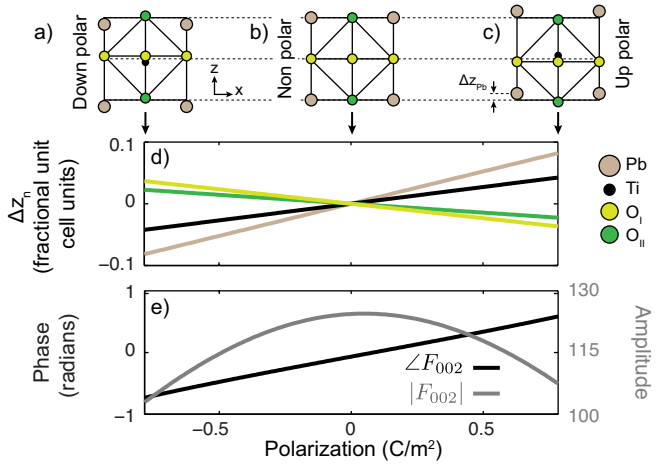

FIG. 3. The unit cell structures of $PbTiO_3$ corresponding to fully compensated bulk polarization in the "down" (a) and "up" (c) states are shown as they appear relative to each other across a 180° domain wall, as calculated from *ab initio* theory [29]. (b) The centrosymmetric reference structure. The ionic displacements Δz_n and the unit cell structure factor F_{002} are plotted vs. polarization in (d) and (e).

The relationship in Fig. 3(e) provides a means to convert the phase of the BPP reconstruction to units of out-of-plane film polarization, as shown in Fig. 4(a). In this image, the aspect ratio has been scaled by a factor of 3 in the y direction to account for the difference between the detector point of view (as reconstructed with BPP) and the film-normal point of view. A line profile across the stripes is shown in Fig. 4(c), together with lines indicating the average polarization magnitude of the film as determined by the specular CTR ($|P| = 0.69$ C/m^2). The two independent analyses of global and nanoscale polarization are consistent, as the polarization of the stripe domains oscillates within the envelope given by the CTR measurement. Therefore, BPP provides a new approach to quantitative ferroelectric domain imaging in epitaxial thin films that can be directly compared with complementary polarization mapping techniques.

Prior to the BPP experiment, calibrated PFM measurements

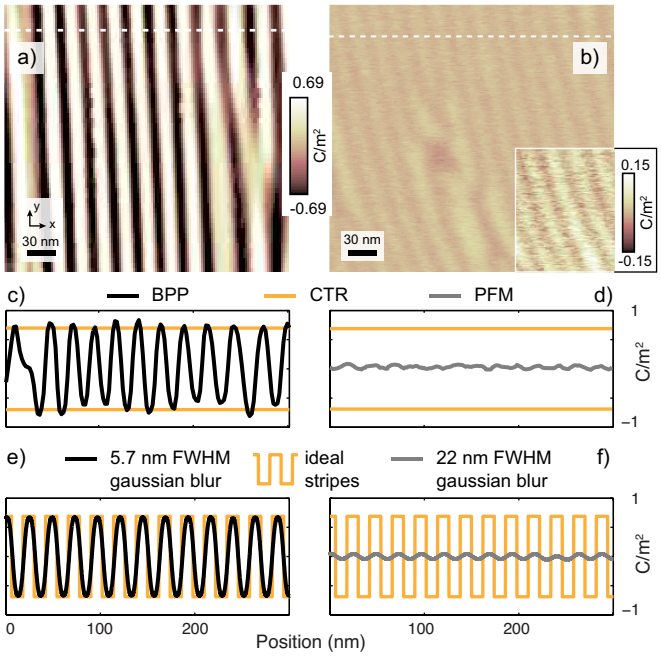

FIG. 4. (a) The stripe domain polarization map generated from the phase of the BPP reconstruction is shown, along with a polarization map measured with PFM in (b). The images show different regions of the sample but share the central color scale (with the exception of the inset in (b), which uses the righthand scale). Profiles taken along the white dotted lines in each image are plotted below the corresponding image, in (c) and (d). The horizontal lines in (c)-(f) represent the average polarization state of the film ($\pm$ 0.69 C/m^2) as determined from the CTR. By fitting such line profiles, the spatial resolutions of these BPP and PFM measurements were determined to be 5.7 nm and 22 nm, and the effect of these resolution functions on idealized stripe domains with $\Lambda = 23$ nm is shown in (e) and (f).

of the surface of this thin film were performed, and a representative area is shown in Fig. 4(b), with the same quantitative color scale as Fig. 4(a). The effective piezoresponse was calibrated using the sensitivity obtained by a force-distance curve, which was used to convert the effective piezoresponse to polarization using the equations and parameter values in the literature [34–37]. Both images, though not of the same area, show similar qualitative stripe domain behavior and morphology. Generally, the stripes display a pronounced tendency to align normal to the substrate surface miscut direction, consistent with previous observations in this thin film system [13]. Though they are predominantly straight and regularly spaced ($\Lambda_{BPP} = 23.5$ nm, $\Lambda_{PFM} = 23.0$ nm), several domains with varying widths and irregular features are seen in both images, possibly due to the local details of the substrate surface beneath the film. We attribute the different ratios of up to down domain area in the two images to differences in pre-image sample processing and to differences in imaging environment (ambient conditions for PFM, and 1.8×10^{-5} Torr vacuum for BPP), which affects the compensation at the top interface of the film [12, 38]. Otherwise, the two techniques provide self-consistent information about the polar domain structure and stripe period in the film. However, we find that polarization in the $\sim$ 12-nm-wide stripes is better resolved by BPP.

In epitaxial $PbTiO_3$ thin films on $SrTiO_3$, 180° domain wall widths have been shown to be very narrow, of order 0.5 nm [3], such that they can be treated as perfect vertical interfaces in the nanoscale imaging experiments done here. Line profiles of the BPP and PFM images like those shown in Figs. 4(c) and (d) can therefore be used to estimate the resolution of the respective images by fitting these types of profiles to an oscillatory box function representing idealized stripes with sharp domain wall interfaces convolved with a gaussian. The resolutions were found to be 5.7 nm and 22 nm respectively (gaussian full width at half max), consistent with the q-limited maximum resolution for BPP of 4 nm, and consistent with typical spatial resolutions of PFM in ambient conditions with Pt-coated tips [39]. We note that two factors that contribute to the lower PFM resolution are the voltage drop across the contact between the tip and the film, as well as the inhomogeneous electric field profile in the film [40, 41]. The effect of the resolution functions of both techniques is shown in Fig. 4(e) and (f), in agreement with the image line scans. With sub-domain size spatial resolution, the BPP measurement can accurately quantify the spontaneous polarization within individual stripe domains.

The high resolution of the BPP image demonstrated here was made possible by the orientation of the stripes relative to the incoming beam. Since the reconstructed image is a projection through the film thickness along the direction of the diffracted exit beam, domains oriented away from the scattering plane will be blurred, and will become irresolvable when oriented normal to it. These limitations can be overcome either by scanning the same area from a number of view points, or by extending Bragg projection ptychography to 3D Bragg ptychography [42]. These approaches involve more complex experiments with longer data acquisition times, but they have the potential to map local polarization in nanoscale domains in three dimensions.

We have demonstrated that x-ray Bragg projection ptychography can be used to quantitatively image a selected component of polarization in epitaxial thin film ferroelectric domains, enabling high resolution nondestructive visualization of stripe domains in complex environments and under buried boundary conditions (e.g. ferroelectric / dielectric superlattices [43, 44]). With further development, Bragg ptychography techniques can potentially resolve the full polarization vector at the nanoscale, providing unique opportunities to address outstanding challenges of domain and domain wall engineering in complex ferroelectric and multiferroic thin film systems.

This work, including use of the the Center for Nanoscale Materials and the Advanced Photon Source was supported by the U. S. Department of Energy, Office of Science, Office of Basic Energy Sciences, under Contract No. DE-AC02-06CH11357. S.O.H., M.J.H., D.K., C.M.F., S.H., and P.H.F. were supported by U.S. DOE, Basic Energy Sciences, Materials Sciences and Engineering Division.

[1] G. Catalan, J. Seidel, R. Ramesh, and J. Scott, Rev. Mod. Phys. **84**, 119 (2012).
[2] D. Fong et al., Science **304**, 1650 (2004).
[3] C.-L. Jia et al., Nature Mater. **7**, 57 (2007).
[4] C. T. Nelson et al., Nano Lett. **11**, 828 (2011).
[5] S. V. Kalinin et al., Annu. Rev. Mater. Res. **37**, 189 (2007).
[6] M. Park et al., Appl. Phys. Lett. **97**, 112907 (2010).
[7] S. O. Hruszkewycz et al., Nano Lett. **12**, 5148 (2012), and associated Supplemental Information.
[8] D. G. Schlom et al., Annu. Rev. Mater. Res. **37**, 589 (2007).
[9] M. J. Highland et al., Phys. Rev. Lett. **107**, 187602 (2011).
[10] G. Stephenson et al., Physica B-Condens. Matt. **336**, 81 (2003).
[11] G. B. Stephenson and K. R. Elder, J. Appl. Phys. **100**, 051601 (2006).
[12] S. Streiffer et al., Phys. Rev. Lett. **89**, 067601 (2002).
[13] C. Thompson et al., Appl. Phys. Lett. **93**, 182901 (2008).
[14] R. Takahashi, O. Dahl, E. Eberg, J. K. Grepstad, and T. Tybell, J. Appl. Phys. **104**, 064109 (2008).
[15] R. P. Winarski et al., J. Synchr. Rad. **19**, 1056 (2012).
[16] The Hard X-ray Nanoprobe beamline is operated by the Center for Nanoscale Materials at the Advanced Photon Source.
[17] The sample was annealed in an oxygen atmosphere at 500° C for several minutes. These are equilibrium conditions for the β stripe phase in (001) $PbTiO_3$ films on (001) $SrTiO_3$, as detailed in Reference [12].
[18] A. Ying et al., J. Appl. Cryst. **43**, 587 (2010).
[19] I. Vartanyants and I. Robinson, J. Phys. -Condens. Matt. **13**, 10593 (2001).
[20] M. Dierolf et al., New J. Phys. **12**, 035017 (2010).
[21] S. O. Hruszkewycz et al., Opt. Lett. **36**, 2227 (2011).
[22] J. M. Rodenburg and H. M. L. Faulkner, Appl. Phys. Lett. **85**, 4795 (2004).
[23] P. Thibault, M. Dierolf, O. Bunk, A. Menzel, and F. Pfeiffer, Ultramicrosc. **109**, 338 (2009).
[24] P. Godard, M. Allain, V. Chamard, and J. Rodenburg, Opt. Expr. (2012).
[25] B. E. Warren, *X-ray Diffraction*. (Dover, New York, 1990).
[26] I. K. Robinson and R. Harder, Nature Mater. **8**, 291 (2009).
[27] E. Fohtung et al., Appl. Phys. Lett. **101**, 033107 (2012).
[28] F. Jona and G. Shirane, *Ferroelectric Crystals*. (Dover, New York, 1993).
[29] B. Meyer and D. Vanderbilt, Phys. Rev. B **65**, 104111 (2002).
[30] D. Fong et al., Phys. Rev. B **71**, 144112 (2005).
[31] G. Saghi-Szabo, R. E. Cohen, and H. Krakauer, Phys. Rev. Lett. **80**, 4321 (1998).
[32] J. Y. Jo et al., Nano Lett. **11**, 3080 (2011).
[33] The anomalous contributions to the atomic form factors at 9.5 keV account for a $\sim$ 4% difference between the $|F_{002}|$ of up and down domains, which is not resolved in the BPP reconstruction.
[34] S. Hong et al., J. Appl. Phys. **89**, 1377 (2001).
[35] D. Damjanovic, Rep. Progr. Phys. **61**, 1267 (1998).
[36] S. Kalinin and D. Bonnell, Phys. Rev. B **65**, 125408 (2002).
[37] O. Dahl, J. K. Grepstad, and T. Tybell, J. Appl. Phys. **103**, 114112 (2008).
[38] R. V. Wang et al., Phys. Rev. Lett. **102**, 047601 (2009).
[39] B. Rodriguez, S. Jesse, A. Baddorf, and S. Kalinin, Phys. Rev. Lett. **96**, 237602 (2006).
[40] S. Hong, J. Woo, H. Shin, E. Kim, K.-H. Kim, J. U. Jeon, Y. E. Pak, K. No, J. Vac. Sci. Technol. B **18**, 2688 (2000)
[41] J. Woo, S. Hong, N.Setter, H. Shin, J.-U. Jeon, Y. E. Pak, K. No, J. Vac. Sci. Technol. B **19**, 818 (2001)
[42] P. Godard et al., Nature Comm. **2**, 568 (2011).
[43] J. Y. Jo et al., Phys. Rev. Lett. **107**, 055501 (2011).
[44] P. Zubko et al., Nano Lett. **12**, 2846 (2012).